MAIN S&T RESULTS/FOREGROUNDS

Wind tunnel tests for drag assessment on both the baseline and optimized tiltrotor configurations

In the first part of the project, wind tunnel tests on a 1/8 scaled, power-off model of the isolated ERICA tiltrotor fuselage (without rotors) in both the baseline and optimized configurations were carried out, with the main objective of accurately measuring drag.
The tests were performed in the RUAG Large subsonic Wind Tunnel in Emmen (LWTE) and they were specifically devoted to assess the benefit of the shape optimization activities on the overall drag of the tiltrotor fuselage. To this purpose, RUAG provided detailed experimental drag benefit measurement between the two configurations "basic" and "optimized". All the optimized components (i.e. nose, wing/fuselage fairing, sponsons and empennage) were tested sequentially with the aim of getting an accurate drag breakdown and identifying the contribution of each component to the overall aerodynamic performance of the fuselage. Initially, for a small number of test cases, the infrared thermography was applied for investigation of the laminar/turbulent transition over the fuselage. Then, transition strips were applied over the models in some locations agreed based on both CFD results and previous experience. Moreover, additional classical flow visualization runs were carried out to enhance knowledge on the transition and separation regions for the different drag reduction configurations.

Model installation
The fuselage model was installed using both a ventral and a dorsal support, in order to quantify strut interference effects on wind tunnel measurements (Figure 1). The strut interference correction was derived from dorsal mount and added ventral dummy strut. While the ventral strut interference was small, the dorsal strut one was large, due mainly to strong interactions with the tail. However, no dorsal dummy strut was used to derive a correction, but a point-to-point correction was applied instead.

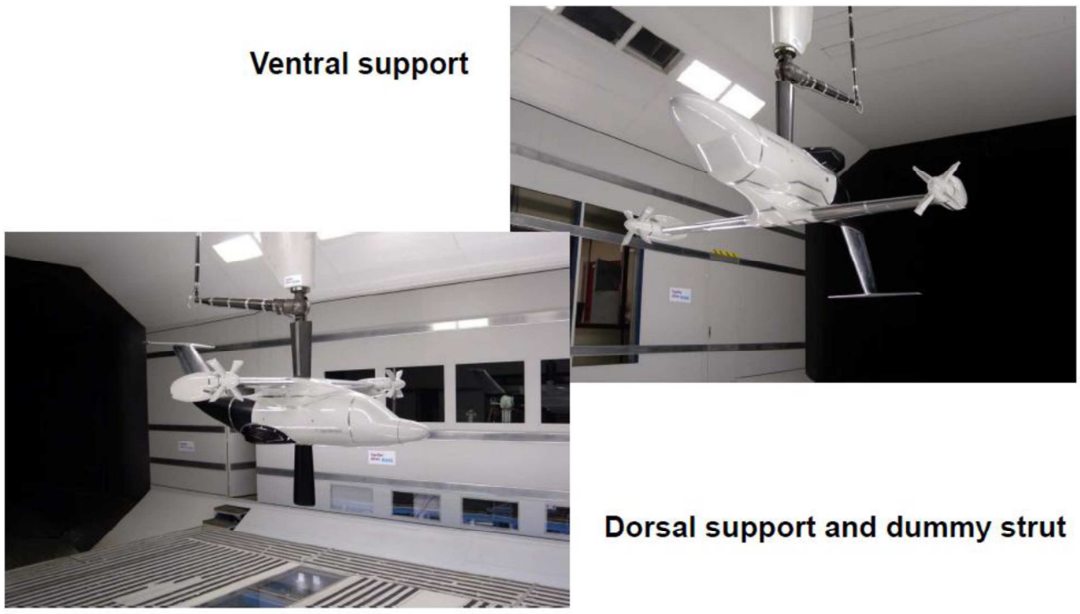

Figure 1: ERICA tiltrotor fuselage installation in the wind tunnel.

Measurements Repeatability
A thorough analysis of repeatability was carried out, and it came out that the experimental results show a good repeatability within 3 drag counts, a result that matches the estimated one before the tests (Figure 2).

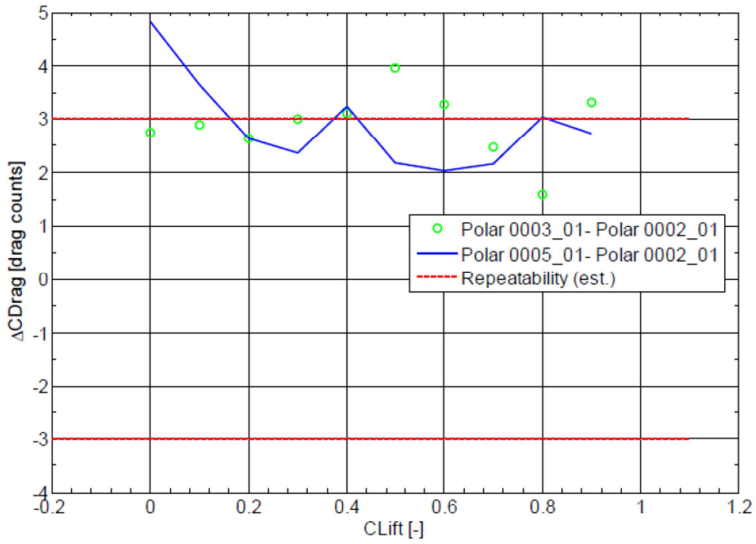

Figure 2: Wind tunnel measurements repeatability estimation.

Laminar/turbulent transition location analysis

The laminar/turbulent transition location over the fuselage nose was analyzed using IR thermography.

In particular, a wide angle IR camera was installed for observation of the upper nose and a telephoto IR camera was mounted on the wind tunnel ceiling for monitoring of the lower portion of the nose. Moreover, variable grain size transition strips were used during the tests and their effect thoroughly assessed (Figure 3).

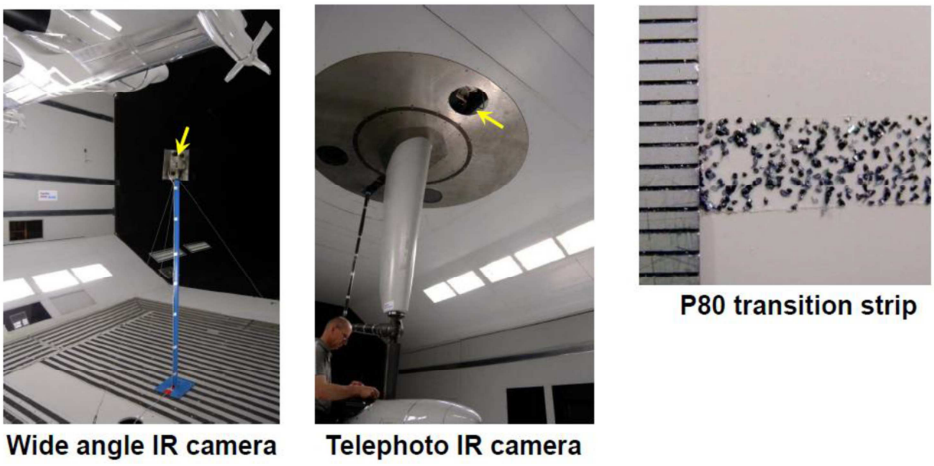

Figure 3: Measurement apparatus for laminar/turbulent transition analysis.

The natural transition on the upper side of both the baseline and optimized nose at an angle of attack equal to 2 deg is shown in Figure 4. The temperature step marking the location of the transition is marked with arrows. It is interesting so see that with the baseline nose, the transition occurs further aft. In both cases, the transition occurs in front of the windscreen. It is likely that the pressure gradient generated by the windscreen is supportive for the laminar-turbulent transition in that area. This is actually consistent with what was found in CFD, as it will be specified later on.

The transition on the upper side of the baseline nose at an angle of attack equal to 2 deg with a P80 transition strip applied is depicted in Figure 5. The transition strip clearly stands out on the thermography picture and is indicated by an arrow . It can be observed that the transition does not happen right at the transition strip, but is rather delayed a little bit. In addition, the “spiky” appearance is caused by turbulent wedges originating from the transition strip, which finally help to trigger the transition also in

circumferential locations that are still laminar otherwise. The influence of the transition strip application on the aerodynamic coefficients of the baseline aircraft was assessed. A significant increase in drag was found for the configurations with transition strips applied. The increase amounts to some 40 to 50 drag counts, depending on lift coefficients. In addition, at fixed AoA, both the lift coefficient and the lift slope show a decrease. Finally, the transition strip application causes a decrease in the pitching moment coefficient.

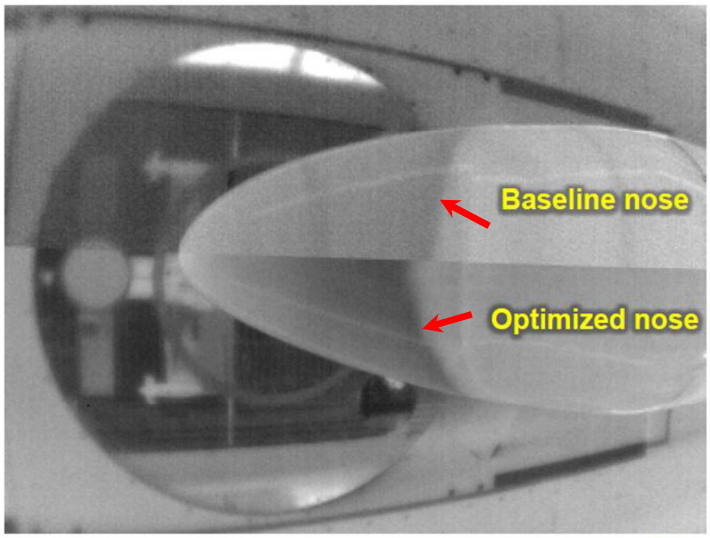

Figure 4: Free transition location on the upper nose for both baseline and optimized nose at AoA= 2 deg.

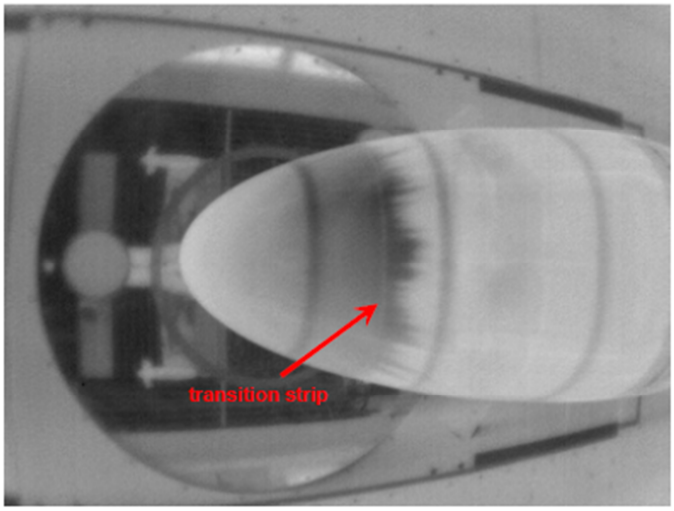

Figure 5: Transition on the baseline nose upper side with P80 transition strip at AoA = 2.0°.

The transition on the upper side of the optimized nose is shown in Figure 6. The location of the transition strip can be seen as a faint line in the picture and is indicated by an arrow as well. Transition occurs aft of the transition strip, with some slight variations visible, depending on circumferential position. Also in this case, an assessment of the transition strip application effect with the aircraft in the fully optimized configuration was carried out. Specifically, regarding the transition strip effects on drag, a drag increase of between approximately 35 to 60 drag counts (depending on lift coefficient) results from the transition strip application. In addition, both lift and lift slope decrease. The pitching moment shows an increase or decrease, depending on the actual lift coefficient.

It was concluded that the transition strip effect on drag and lift is similar for both optimized and non-optimized configurations and of same magnitude for both configurations. Contrary to that, the effect on

the pitching moment shows some differences. However, since most of the optimization analyses were made only for the same types of transition, and with the main focus on drag, this was deemed to be not important for the subsequent analysis.

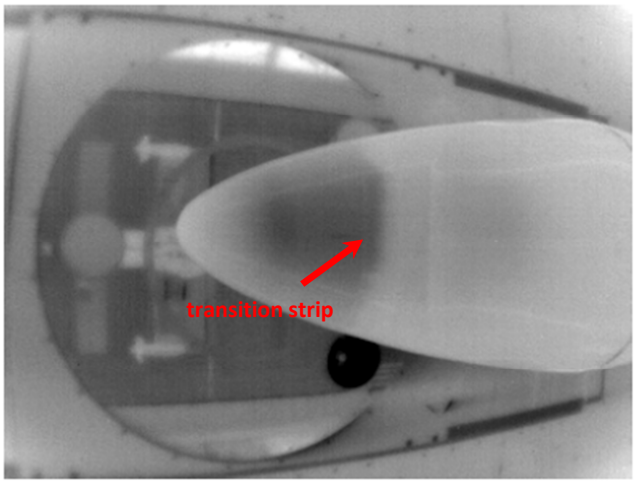

Figure 6: Transition on the optimised nose upper side with P80 transition strip at AoA = 2.0°.

Flow visualization using minitufts

Fluorescent minitufts were used for flow visualization over the rear portion of the fuselage and the sponson surface in a number of test conditions (Figure 7). Ultraviolet lighting was used to illuminate the fluorescent tufts, giving enough contrast for video recording. Acquired data were used for validation of numerical results and assessment of vorticity production of both the baseline and optimised sponson shapes.

One of the great advantages of minitufts is that their intrusiveness can often be neglected, so that visualizations can be performed at the same time as force measurements are taken.

In particular, a series of tests without minitufts were carried out first on both the baseline and optimized fuselages, and then the same tests were carried out with minitufts applied in order to evaluate interference effects. Since, as expected, interference was negligible, these devices were kept applied over the fuselage during the overall wind tunnel campaign.

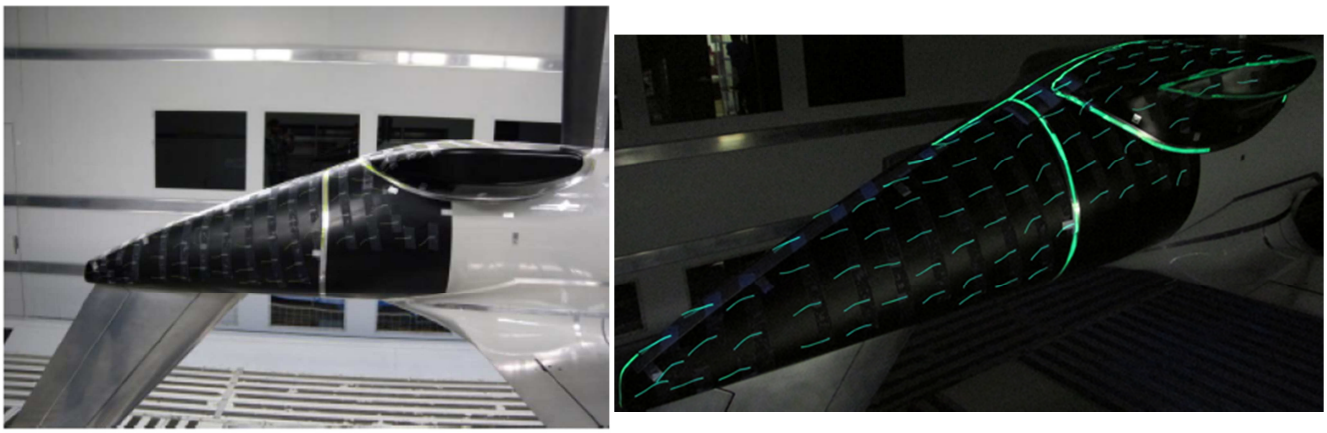

Figure 7: Flow visualization using minitufts on the rear fuselage.

Force measurements and analysis of optimization results

To assess the benefits of optimized components in terms of drag reduction, the measurements with and without said optimized component was compared by calculating the difference between the measurements. Actually, two different kinds of (mainly drag) wind tunnel data comparisons were made:

- **Fixed lift:** For a fixed lift comparison, the measured data was interpolated to the same lift coefficient values. The reason for making this kind of comparison was that, in reality, the lift is given by the flight condition, namely it is equal to the weight for a steady horizontal flight. So if an optimization results in a difference in both drag and lift, the AoA must be adjusted to keep the lift coefficient the same.
- **Fixed AoA:** The numerical optimization of the aircraft components was carried out at one design point with a fixed angle of attack. To be in line with the CFD results, it was therefore necessary to also compare the optimization results at this fixed AoA. For this purpose, the measured data was interpolated to the same AoA. The design AoA used for optimization is $\alpha = -1.97°$.

- **Optimized nose**: It was found that the effect on lift and especially drag was beyond the accuracy of the measurement setup. However, a more or less lift-independent increase in pitching moment was observed.
- **Optimized wing/fuselage junction**: The drag improvements resulting from the optimized wing-fuselage faring are strongly dependent from the actual lift coefficient. In fact, there is a drag reduction near the design point, but with increasing lift coefficient the improvement goes to zero, and at higher lift coefficients, there is even a drag penalty resulting from the optimized wing-fuselage fairing. In addition, a decrease in both lift and lift slope can be seen. With non-null sideslip angle, the amount of lift decrease becomes smaller. Contrary to the optimized nose, the optimized wing-fuselage fairing causes a decrease in pitching moment, which gets larger at higher lift coefficients.
- **Optimized sponson**: The effect of the optimized sponsons was measured in both the ventral and dorsal mount configuration of the aircraft. A significant drag reduction was measured accompanied with a minor lift reduction and a slight increase in pitching moment. Concerning the drag reduction, the ventral and dorsal data agrees very well for zero and -5° of sideslip. However, for the -10° sideslip case, a discrepancy becomes visible, with the drag reduction in the ventral case being visibly larger than in the dorsal case. This might be related to the interference of the wake of the strut with the flow around the sponsons.
- **Optimized empennage**: The effect of the optimized empennage has not been measured directly, only the combined influence of both optimized sponsons and empennage was available. In order to assess the impact of the empennage configuration alone it was necessary to remove the sponson effect from the analysis. This was accomplished by first calculating a new virtual polar based on the sponson effect and a baseline polar. It was found that there is some slight improvement in drag visible with the optimized empennage. However, the improvement is quite small and at the limit of the repeatability of the test. The impact on lift is comparably small. As expected, the impact on the pitching moment as is the largest. At lower lift coefficients, the pitching moment increases, while at higher lift coefficients, a decrease becomes visible.

Globally, it was found that the combined effect of all optimized components results in a drag reduction of 32.8 to 35.8 drag counts at the design AoA of -1.97°. This equals a drag reduction of 4.19% to 4.57% relative to the unmodified baseline configuration. The corresponding values are 27.7 to 31.2 drag counts and 3.53% to 3.97% when comparing at constant lift (Figure 8).
Comparing the design AoA case and the fixed lift case, it can be seen that the drag reduction is larger in case of the fixed AoA, but the optimized configurations is showing a lift loss. That is why the drag reduction

is smaller in the fixed lift case, since increasing the lift coefficient to its original value does result in an increase in induced drag.

The largest single contribution comes from the optimized sponsons, followed by the optimized wing/fuselage fairing. However, the wing-fuselage fairing causes also a significant loss of lift at the design AoA.

The drag reduction due to the optimized empennage and especially due to the optimized nose is very small, partly even beyond the repeatability of the test. The optimized nose causes a significant increase in pitching moment. Also other components have an impact on the pitching moment and thus the effect of trim drag should be considered as well for a final assessment of the drag reduction potential.

Finally, it was concluded that the most promising single component in terms of drag reduction, with only minor impacts on lift and pitching moment, is the optimized sponson.

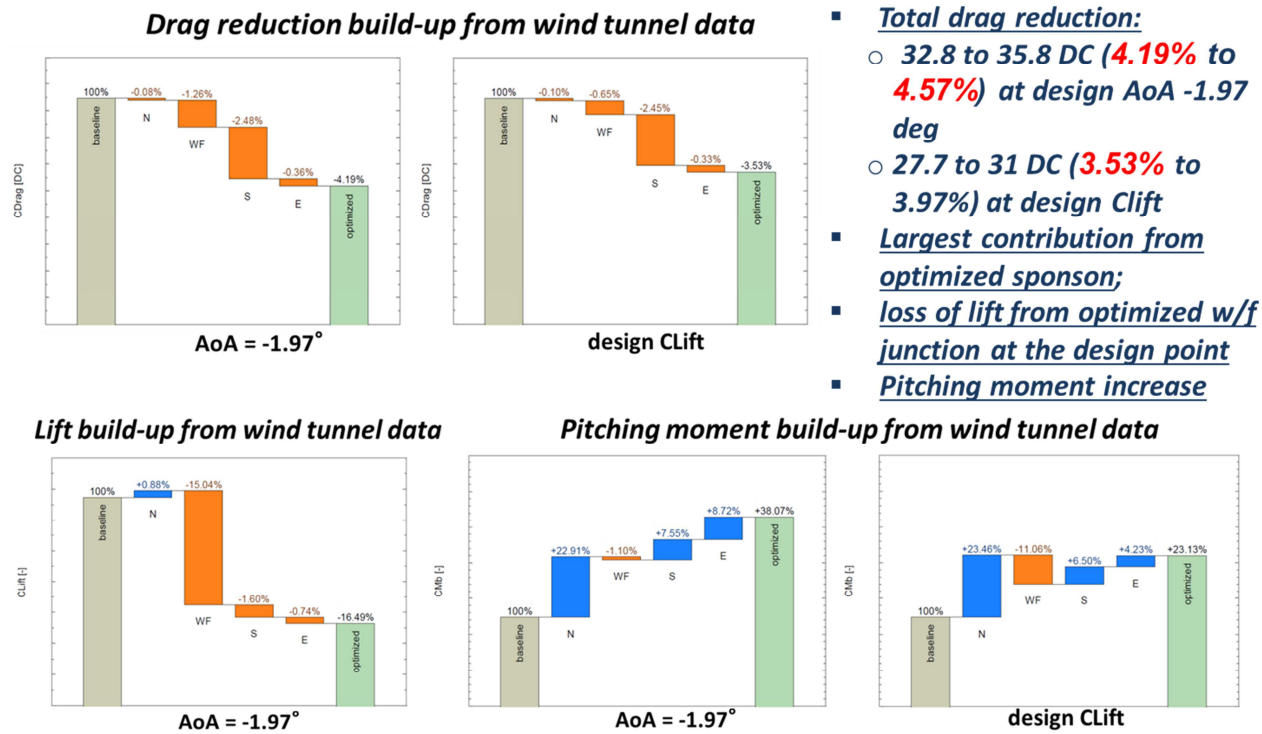

Figure 8: Drag, lift and pitching moment build-up from wind tunnel results at both fixed AoA and lift coefficient.

PIV measurements

In addition to the global force measurements, and for a limited number of cases, the wake downstream of the landing gear sponsons was measured by Stereo Particle Image Velocimetry technique (S-PIV), even though this activity was not fromally included in the project (Figure 9). Actually, the PIV campaign was carried by CIRA using some additional budget made available by GRC. Additional CFD runs were then carried out by HIT09 to support the PIV campaign (Figure 10).

The flow structures were analyzed in relation to the drag reduction observed for the optimized sponsons in comparison to the baseline configuration. The three velocity components of the flow field obtained from measurements provided a localized validation of the CFD tools adopted in the optimization phase. These wake flow measurements were carried out to better understand the flow mechanism responsible for the

benefits observed for the new optimized sponsons. The measurements were carried out at five different vertical cross planes at different distances from the model nose (Figure 9).

Figure 9: PIV tests over the ERICA fuselage.

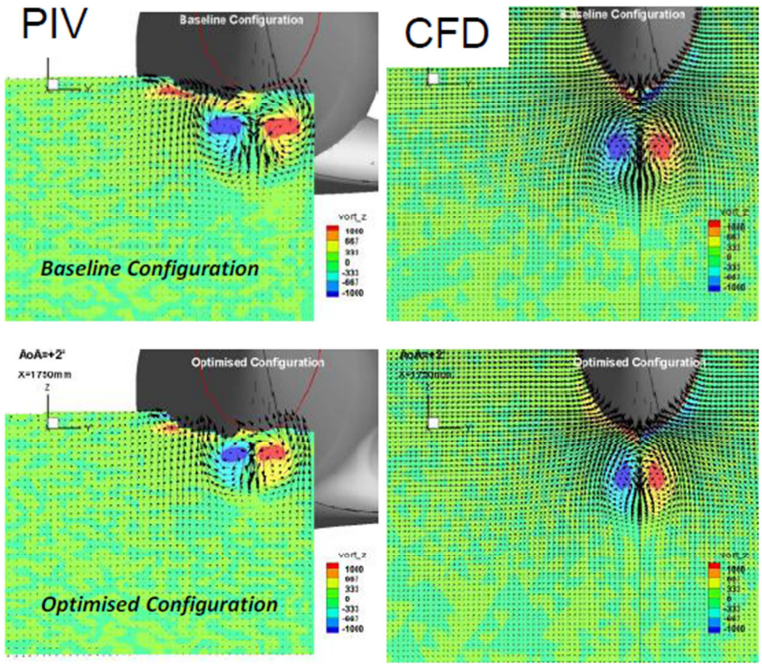

Figure 10: PIV/CFD vorticity contour map over one PIV measurement plane on both baseline and optimized sponson.

The S-PIV wake characterization was performed at constant flow speed for different fuselage attitude and yawing angles.

The measured velocity fields showed a couple of contra rotating vortices shedding downstream of the fuselage sponsons. From the PIV (coupled with CFD data) the following conclusions were drawn:

1. The flow field measurements indicate a clear wake reduction in terms of size and momentum loss, of the order of about 2% of the flow rate ratio. Furthermore the vortex shedding for the optimized sponsons is delayed compared to the baseline, and the wake remains closer to the fuselage body.
2. The out of plane vorticity showed a notable intensity reduction by about 20% to 35% for the optimized sponsons in comparison to the baseline configuration.

3. Considering the effect of the optimized configuration with respect to the baseline, the CFD and the PIV results were similar showing size and vorticity alleviation.
4. A direct CFD and PIV data comparison shows some differences. The wake presents an earlier formation for the CFD results respect to the PIV data. The CFD wake shape is almost elliptical against a less uniform PIV profile. The CFD vortex intensity is smaller of about the 40% respect to the PIV data.
5. The vortex development for the different model attitudes has been measured and vortex growth and the dissipation phenomena can be investigated.
6. A valuable contribution to the experimental data base has been generated with the flow field measurements for future comparison with CFD simulations.

Additional CFD simulations are foreseen in order to take into account the unsteadiness of the flow field and to allow better comparisons with the experimental data.

Brief description of the optimization methodology

The optimization procedure used by HIT09 and University of Padova in a previous CfP (namely CODE-Tilt) for identifying the optimal shapes of the tiltrotor fuselage components is basically structured in three phases (Figure 11):

1. Baseline model preparation and simulation phase;
2. Automatic optimization phase;
3. Post-processing.

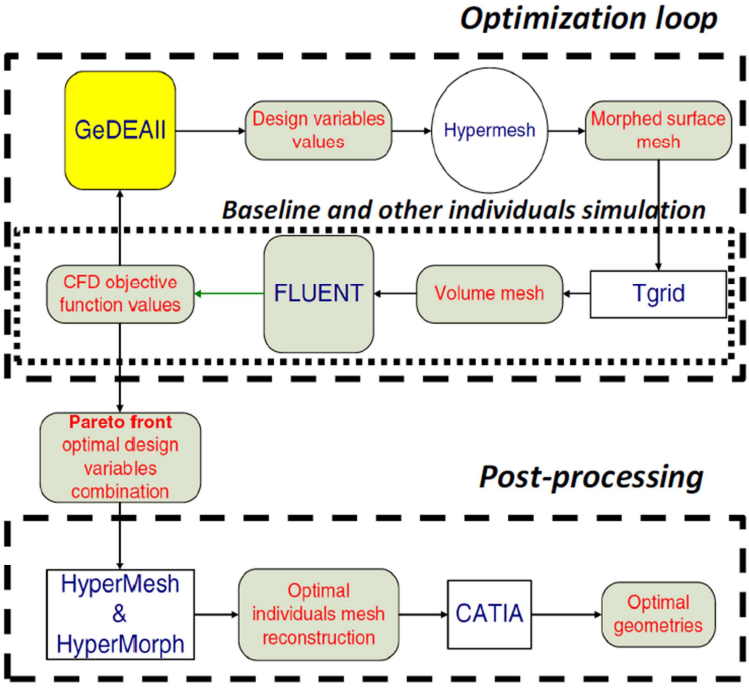

Figure 11: Optimization method flow-chart.

Baseline model simulation

Typically the starting point is represented by the CAD model of the baseline configuration (Dassault Systemes CATIA® V5 was chosen for the present application). Starting from the geometrical model, the procedure moves into the "baseline simulation block", where the baseline configuration of the component under consideration is analyzed, in terms of aerodynamic performance in the most relevant operating

conditions, via CFD computation using the selected flow solver. The assessment of the baseline solution allows the designer to properly understand the flow field characteristics of the object under analysis. Specifically, it gives fundamental indications for the optimization objectives and constraints identification and allows to properly set up the geometrical parametric model.

Automatic optimization execution

Once the preliminary operations are completed, the automatic optimization loop starts (Figure 11): the procedure is made up by the following components:

1. GDEA (Genetic Diversity Evolutionary Algorithm): it is an advanced multi-objective optimization algorithm based on evolutionary techniques developed at the University of Padova and it acts as the optimization engine;
2. Altair HyperMorph®: it allows the conversion of design parameters selected by GDEA into morphed CFD cases, suitable for objective function evaluation;
3. Ansys Fluent®: the selected flow solver; it takes as an input the morphed CFD cases coming from HyperMorph® and gives back to GDEA the correspondent values of the selected objective functions.

During the optimization process, GDEA lets a population of individuals (each one corresponding to a different set of design variables and so to a different geometry configuration) "evolve" until the convergence to the Pareto optimal frontier has been reached. The Pareto frontier represents the solution of a multi-objective optimization problem, and is made up of a set of so-called "non-dominated" solutions. A non-dominated solution is one in which an improvement in one of the objectives necessarily requires the degradation of another.

Post-processing

The Pareto frontier, which is the output of the automatic optimization loop, represents a multiple set of solutions equally optimal according to the Pareto concept, but of course different from the aerodynamic and engineering point of view. Indeed, each solution over the Pareto frontier may present advantages and drawbacks with respect to the other solutions. In order to identify, among the optimal set, the most appropriate design, a post-processing activity is necessary. Thanks to the intrinsic multi-objective approach adopted, the designer is allowed to select, among the Pareto optimal set, the solution which is most suitable for his/her needs: for example, choosing to privilege the improvement of one objective with respect to another or even including other considerations such as non-aerodynamic requirements. The strength of the selected approach is that the designer can choose the proper trade-off between the objectives when the optimization work has been completed and he is not forced to introduce his arbitrariness in the problem set up, as commonly happens using traditional optimization approaches.

CFD analysis of the optimized model scale configuration in wind tunnel conditions

A thorough CFD campaign was carried out over the 1/8th scaled ERICA fuselage at wind tunnel conditions with the aim of fully validating the numerical models to be subsequently used for evaluation of optimization effects at full scale conditions. This CFD campaign included also some investigations on the numerical modelling of laminar/turbulent transition.

Validation of laminar/turbulent transition numerical modelling against literature cases

A series of simulations were carried out aimed at assessing CFD transition modeling to be successively applied to the tiltrotor fuselage in order to identify proper locations for the transition strips. Specifically,

CFD transition modeling needed to be validated against data published in the literature for different Reynolds numbers. The estimation of the transition location was carried out using the criterion introduced by Menter: to this purpose, the distribution of both skin friction coefficient and turbulent intermittency was monitored so as to determine where a sudden increment of these quantities is evidenced. In DREAm-TILT, it was agreed that validation of the CFD transition modelling was to be carried out using some data published in the literature and regarding transition on a simple three-dimensional body over a range of different Reynolds number.

In order to validate the transitional model of Menter, results obtained during an the experimental campaign conducted at NASA Langley research center were taken as reference. The considered experimental campaign provides very useful results about laminar-to- turbulent transition occurring on a dirigible wind tunnel model. In particular, one flight condition was thoroughly investigated, for which is the transition location is specified as a function of the body axial coordinate. Several data, concerning drag values, transition location and boundary layer development along the fuselage surface is available. These results were considered for validation purposes.

A series of simulations at different Reynolds numbers were carried out on the so-called “Akron” airship, once a reliable numerical model was identified in terms of both mesh settings and simulation parameters, especially regarding the turbulence specification method. The final selected numerical set-up gave good results at all the tested Reynolds regimes, both in terms of transition location and drag coefficient.

Moreover, the same numerical settings were applied on a spheroid, over which experimental wall shear stress values at five Reynolds numbers and at different incidence angles were available. Also in this case, results were satisfactory: in particular, the transition onset was predicted with good accuracy at varying Reynolds number and at null incidence angle. Further simulations of transition on spheroid at non-null incidence angle and correlation against experiment were carried out. In this case, correlation of numerical wall shear stress profiles with experiment was not satisfactory at all. In particular, the transition front predicted by CFD was much more inclined with respect to the free-stream velocity direction than the experimental one. A series of analyses were carried out over the case at alpha=2.5 deg, in order to further assess sensitivity of results to computational mesh parameters and CFD simulation settings. In addition, also an unsteady simulation was carried out in order to verify if an unsteady analysis of the evolution of the transition curve over the spheroid could give a better correlation with experiment. However, the numerically predicted transition curve was found to be quite insensitive to all the modifications to the numerical model, and correlation with experiments was always poor.

In light of the scarce correlation with experimental data on transition that was found using the Menter-Langtry model over the spheroid at non-null incidence angles, a bibliographic review was carried out in order to find other numerical studies regarding transition and compare them with obtained findings. To this purpose, it was found that the influence of model specific parameters, e.g. the turbulence intensity and the turbulent to molecular viscosity ratio on the transition locations predicted using the Menter model is remarkable. For this reason, some modifications were necessary to be applied to the original transition model in order to improve prediction capabilities. Moreover, it was observed that, once the given flow conditions lead to three-dimensional transition phenomena, the transition prediction with the Menter model is not reliable, because the model is based on the characteristics of two-dimensional boundary layers and three-dimensional transition mechanisms are not taken into account. In particular, results over the spheroid are very similar to those found in the numerical simulations carried out by HIT09 and University of Padova, and they demonstrate that the capabilities of Menter model for such cases are insufficient and no reliable transition locations may be obtained.

1/8 Scale model characterization

An extensive numerical simulation campaign was carried out over the 1/8th scaled ERICA tiltrotor fuselage aimed at identifying suitable numerical models of both the baseline and optimized tiltrotor fuselage geometries and validating them against wind tunnel data. Specifically, a series of CFD analyses were carried out in wind tunnel conditions and obtained results were analyzed in terms of flow distortion, total pressure losses, flow separation and all those aspects that may affect the efficiency of the ERICA fuselage.

The support system was included in the numerical model either in the ventral or dorsal mode, depending on the test case, in accord with the experimental test matrix carried out in the RUAG wind tunnel. For each geometrical configuration, the aircraft pitch attitude was varied from -18° to 18°. In addition, a limited number of simulations at non-zero sideslip angles were carried out (yaw attitude was varied from 0° to 10°). The wind tunnel model was created using the actual LWTE cross-section shape and size, while along the longitudinal direction the length was established based on previous experience that suggests an extension of the fluid domain 2÷3 aircraft lengths upstream and 5÷6 lengths downstream of the fuselage. A view of the model inserted in the wind tunnel with both ventral and dorsal struts is show in Figure 12.

The numerical mesh was built up using Hypermesh® and it was of the hybrid type (Figure 13): prismatic layers were created over the aircraft and pylons surfaces in order to better resolve the boundary layer, while tetrahedral elements were used in the rest of the fluid domain. The overall mesh size was 16.2 M elements (on one half aircraft). Ansys Fluent® was used as the CFD solver: steady simulations were carried out, using k-ω SST turbulence modeling with specification of turbulent intensity and hydraulic diameter.

The same analyses were performed on the optimized configurations as well, in order to guarantee that the effects of shape modifications coming out from the optimization process were evaluated with the required level of accuracy. Specifically, all the "intermediate" optimized configurations were analyzed, with the optimized components mounted one at a time on the fuselage, in order to replicate the wind tunnel measurements and get a deeper insight into the interference effects of the various components. Specifically, the analyzed components were: nose, wing-fuselage junction, sponsons and empennages.

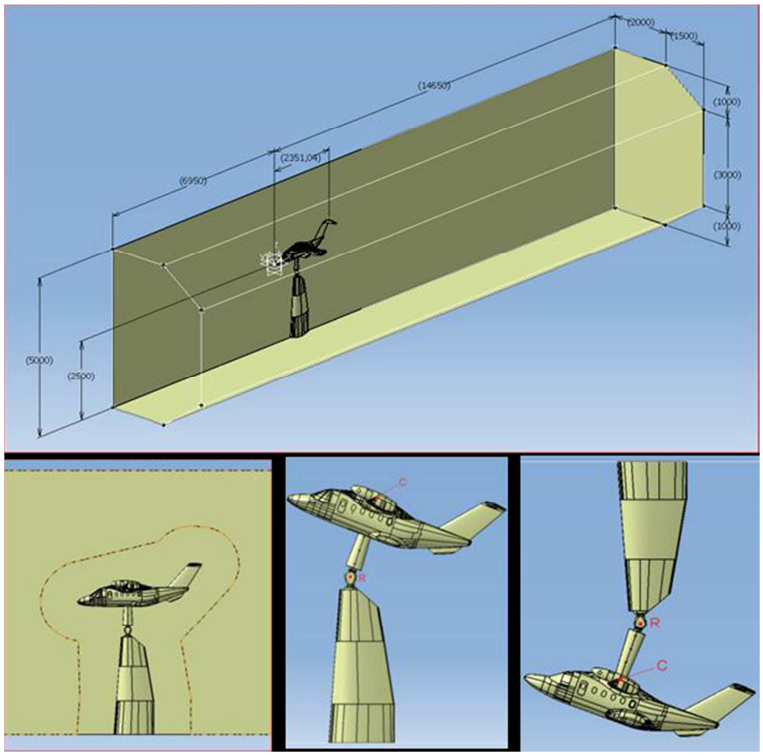

Figure 12: ERICA model inside the wind tunnel with both ventral and dorsal struts.

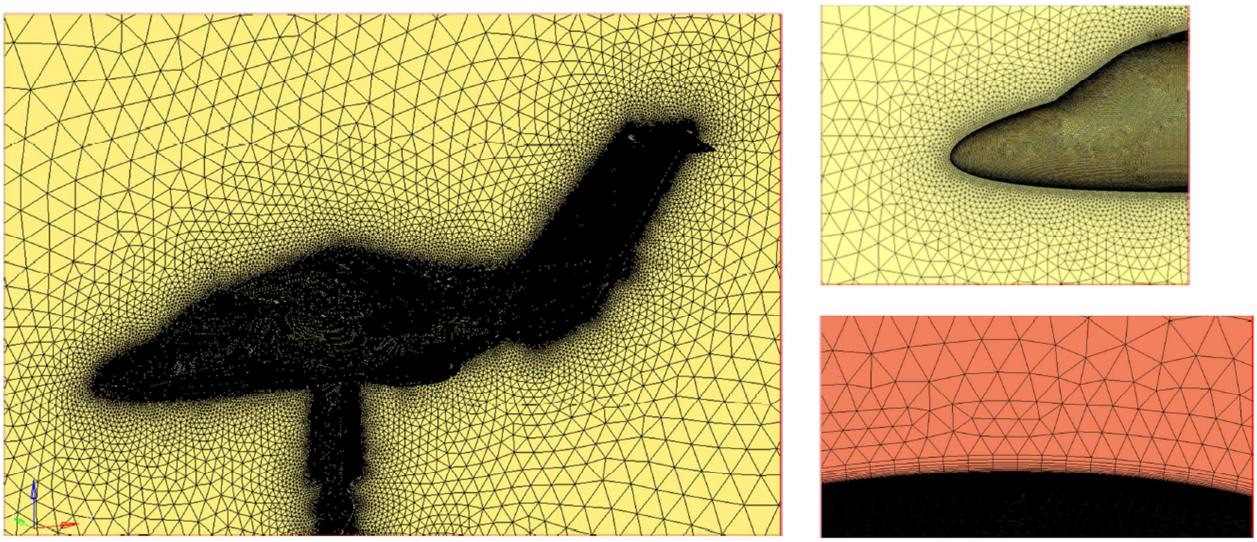

Figure 13: Overview of the computational mesh over the 1/8th scaled fuselage and details of superficial grid and prismatic layers.

Aerodynamic coefficients of the baseline 1/8 scaled tiltrotor model (lift, drag and pitching moment) coming from the CFD simulations are summarized in Figure 14. Experimental data collected during the test campaign were used for direct comparison with CFD results in all the geometrical configurations. Since experimental runs with single optimized components were carried out only with transition fixed, it was decided to compare all the geometrical configurations at fixed transition in order to make them consistent with each other. It is worth noting that the experimental model included the propeller stubs, the effect of which on drag was known from previous experiments; therefore the effect of such stubs were properly taken into account upon comparing numerical vs. experimental data.

Overall, the correlation between experimental and numerical data is very good at low and medium angles of attack, i.e. in the range [-12, +12 deg]. At higher absolute angles of attack, i.e. $\alpha > 12$ deg and $\alpha < -12$ deg, discrepancies are slightly higher, even if still reasonably low. In particular, lift coefficient values are excellently captured throughout the overall range of analysed angles of incidence, except for $\alpha > 12$ deg. For drag, the correlation is very satisfactory in the range [-15, +10 deg], while for $\alpha > 10$ deg. the numerical calculations tend to underestimate the drag relative to experimental data. However, the correlation in the vicinity of $\alpha = -2$ deg, which is the attitude used for optimization, is excellent, and this suggests that the model is reliable as far as the evaluation of optimization effects is concerned. For the pitching moment coefficient, the correlation in the range [-12, +12 deg] is also excellent, with the slope of the linear portion of the curve very well captured, while a degradation of results is apparent at the highest values of incidence angles. In addition, the aerodynamic efficiency of the tiltrotor is illustrated in Figure 14: once again, a very satisfactory correlation with experiment is shown and it can be deduced that the efficiency maximum value is located around $\alpha = 2.5$ degrees.

Regarding the optimized components, the following results were found:

1. regarding the ***nose***, results obtained in wind tunnel conditions are consistent with those achieved during the component optimization. Specifically, a drag reduction is achieved thanks to the optimized nose, accompanied with a simultaneous lift increase. At $\alpha = -1.89$ deg, which is close to the incidence value used for optimization (i.e. -1.97 deg) the drag reduction is equal to 0.25% or 0.16% according to CFD or wind tunnel respectively, with a simultaneous lift increase of 0.35% or 0.94% respectively;

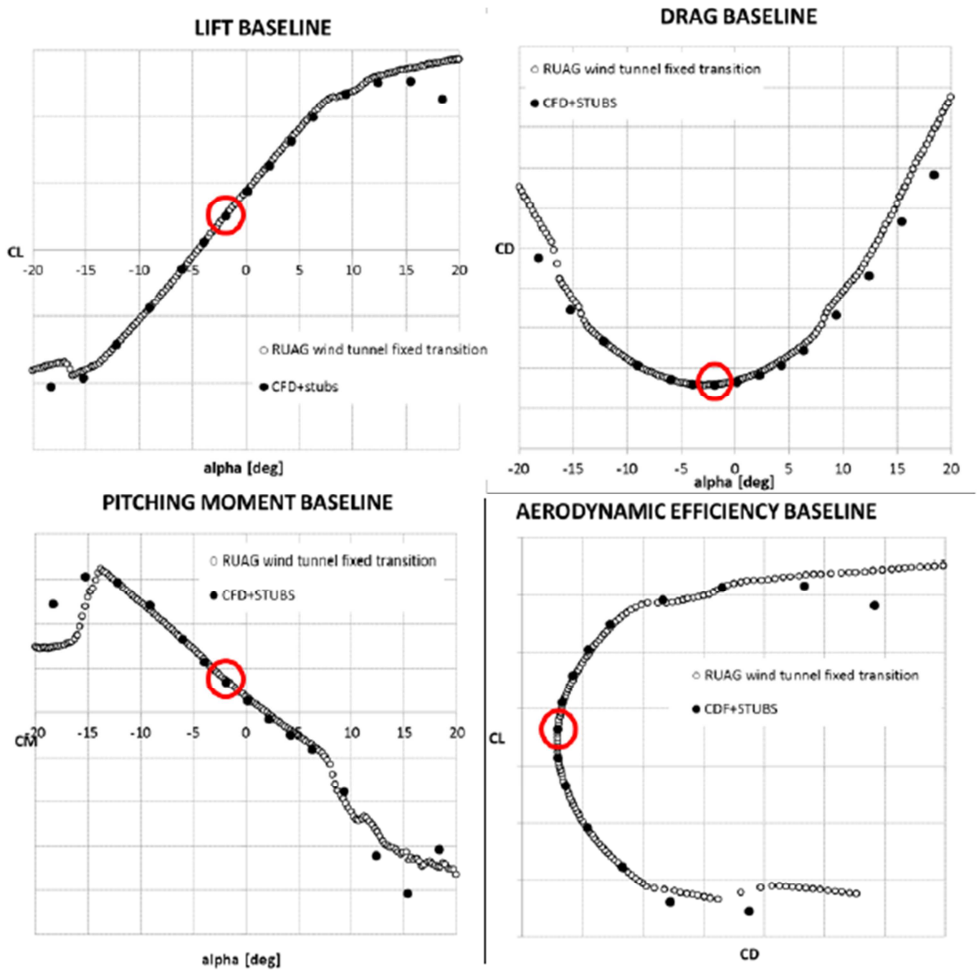

Figure 14: Lift (upper-left), drag (upper-right), pitching moment (bottom-left) and efficiency polars (bottom-right) of the baseline geometry: comparison between the CFD model results and experimental data.

2. as far as the optimized ***wing/fuselage junction*** is concerned, it gives a drag reduction at incidences close to the cruise value. However, this drag reduction is accompanied with a simultaneous lift decrease. In particular, at α =-1.89 deg, the drag reduction is equal to 0.76% or 1.23% according to CFD or wind tunnel respectively, with a simultaneous lift decrease of 16.7% or 14.6%. However, aerodynamic efficiency is increased with respect to the baseline, at least for angles of attack close to the cruise attitude. Results obtained in wind tunnel conditions are in some way consistent with those achieved during the component optimization, but the lift penalization at cruise attitude is magnified in wind tunnel conditions. The lift drop is due to the geometrical differences between the baseline model tested in wind tunnel and that used for optimization. Actually, the lift reduction at cruise condition in the optimized fuselage was originally featured by the baseline fuselage used for optimization as well, so actually optimization itself is not responsible for the observed lift decrease;
3. concerning the optimized ***sponson***, a significant drag reduction, equal to 3.43% or 2.45% was found at cruise attitude according to CFD or wind tunnel respectively, together with a slight lift reduction, equal to 0.83% or 1.75%. A meaningful enhancement was also found in the aerodynamic efficiency. These results are nearly consistent with those achieved during the component optimization, even though the lift penalization at cruise attitude was not found in full scale optimization and drag reduction was higher than the current result;

4. regarding the optimized ***empennage***, a drag reduction of 1.1% was found at cruise attitude according to wind tunnel, while a drag increment of 0.83% was observed from CDF. On the other hand, the lift coefficient is preserved; these results are not consistent with those achieved during the component optimization, since the drag penalization was obviously not found during optimization, being the drag reduction the main objective of optimization;

In Figure 15, the overall effects of the inclusion of all the optimized components are shown: specifically, both CFD and experimental data of the optimized 1/8-scaled fuselage are compared against the baseline. In addition, a zoom of the curves near the optimization attitude (i.e. α=-1.97 deg) is given in the same figure. When for the angles of attack α are close to those used for the optimization, the fuselage features a drag reduction with respect to the baseline equal to 4% and 5% according to CFD or wind tunnel data respectively (percentage values are referred to overall aircraft including the propeller stubs). However, this drag reduction is accompanied with a simultaneous, significant lift decrease. In particular, at α=-1.89 deg, the lift decrease amounts to 17% approximately and 16% according to CFD or wind tunnel data, respectively. It is worth recalling that this lift drop is due to the geometrical differences between the baseline model tested in wind tunnel and that used for optimization, and was already present in the baseline geometry used for optimization, so it is not a direct outcome of the optimization. Despite the significant lift decrease, the aerodynamic efficiency of the optimized fuselage is significantly increased with respect to the baseline (Figure 15), not only at the optimization attitude, but also over the whole low/medium range of incidence angles. Finally, regarding the pitching moment characteristics, the curve slope is increased with respect to the baseline (Figure 15).

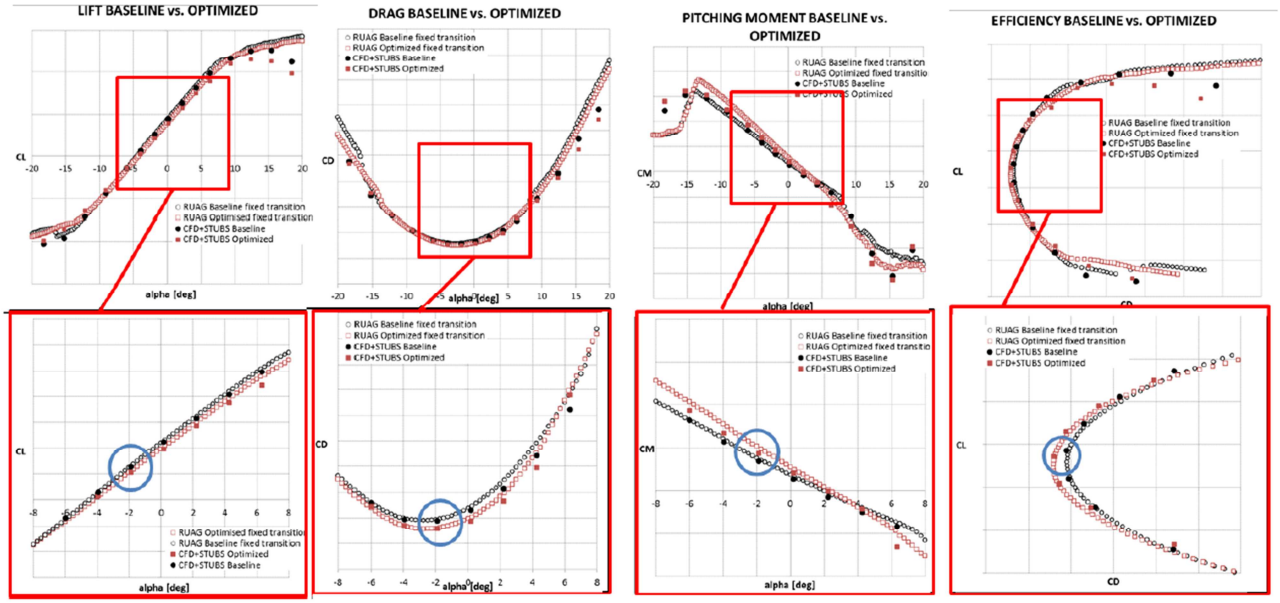

Figure 15: Lift, drag, pitching moment and efficiency polars of the baseline and the optimized 1/8-scaled fuselage geometry: comparison between CFD results and experimental data. Overall polars (top) and zoom around the optimization attitude (bottom).

In Figure 16, a summary of the achieved optimization results in terms of drag reduction is given: in particular, CODE-Tilt and DREAm-TILT results for each optimized component (both numerical and experimental) are reported and compared against the pertinent GRC target. First of all, it has to be noticed that the original drag reduction calculated in CODE-Tilt refers to the aircraft without rotor stubs: since the

stubs contribute to the whole drag in a significant way (around 30% of the total drag), and since they were actually included in the wind tunnel tests, the drag gain coming from optimization was re-calculated including the stubs. As is apparent from the figure, while without stubs the achieved reduction in CODE-Tilt was 7.7%, including the stubs it is reduced to 5.1%. On the other hand, in DREAm-TILT it was found that the overall drag reduction at design incidence is equal to 4% and 5% according to CFD or wind tunnel data respectively. Apparently, in spite of the differences in the results between CODE-tilt and DREAm-TILT, the overall target for drag reduction required by GRC (i.e. 3.55%) is achieved and even exceeded, according to both CFD and wind tunnel results. In addition, the experimentally measured drag reduction (i.e. 5%) is very close to that predicted in CODE-Tilt (i.e. 5.1%) when the stubs effect is included.

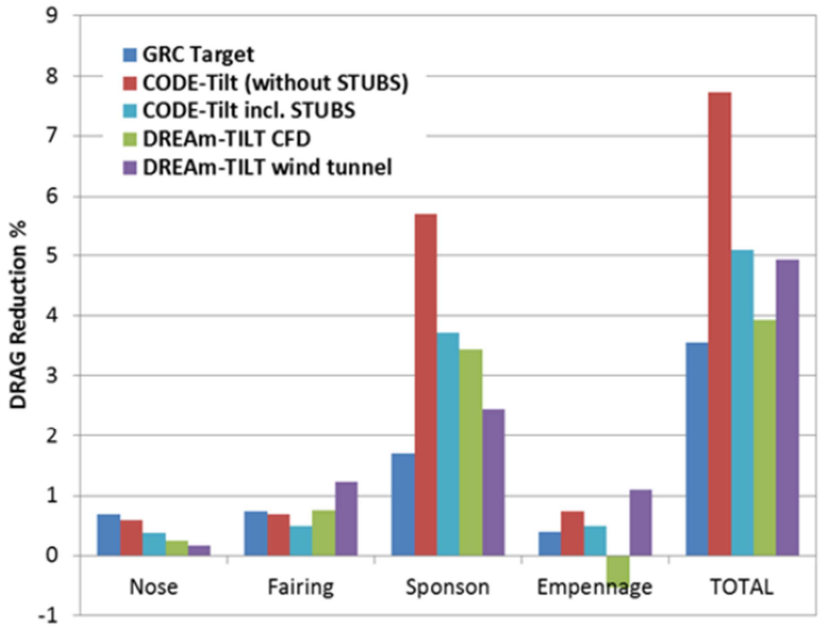

Figure 16: Summary of achieved optimization results in terms of drag reduction: CODE-Tilt and DREAm-TILT results vs. GRC target, numerical and experimental results.

CFD analysis of the optimized full scale configuration including the rotor effects

Starting from the numerical model of the 1/8 scaled tiltrotor fuselage fully validated against wind tunnel data, a deep numerical analysis was carried out over the full scale ERICA fuselage at real flight conditions with the aim of finally assessing the optimization effects at full scale. Hence, Mach and Reynolds number effects were analyzed and also rotor inflow interference was taken into account.

Laminar/turbulent transition location over the tiltrotor fuselage

A series of calculations were carried out at full scale conditions using the laminar/turbulent transition numerical model by Menter. Obtained results were intended to be used for identification of proper locations for the transition strips to be applied over the model during wind tunnel experiments. To this purpose, the same numerical set-up for transition calculation identified over literature cases was applied to both the model scale and the full scale fuselage. However, obtained results were quite misleading. Actually, at model scale conditions transition seems to be located far downstream than expected over all the surfaces of interest. Then, transition onset is very sensitive to turbulent intensity settings (Figure 17). A comparison with experimental data was carried out at an incidence angle equal to 10 deg: in particular,

results were compared against those coming from a flow visualization that was carried out over the tiltrotor wing during a dedicated campaign at Politecnico di Milano wind tunnel, and results at both 0.3% and 1% turbulent intensity seem quite consistent with experimental data, provided that the experimental transition line is correctly interpreted (Figure 18). The same model was applied for simulations at full scale conditions, and in this case it was found that transition occurs very upstream in all the components of interest (i.e. in the first chord percentages of the lifting surfaces), see Figure 19.

Based on these results, it was agreed with AgustaWestland to carry out a comparison with the experimental location of transition strips used in the previous tests over the tiltrotor fuselage and use a best practice, empirical determination of strips location.

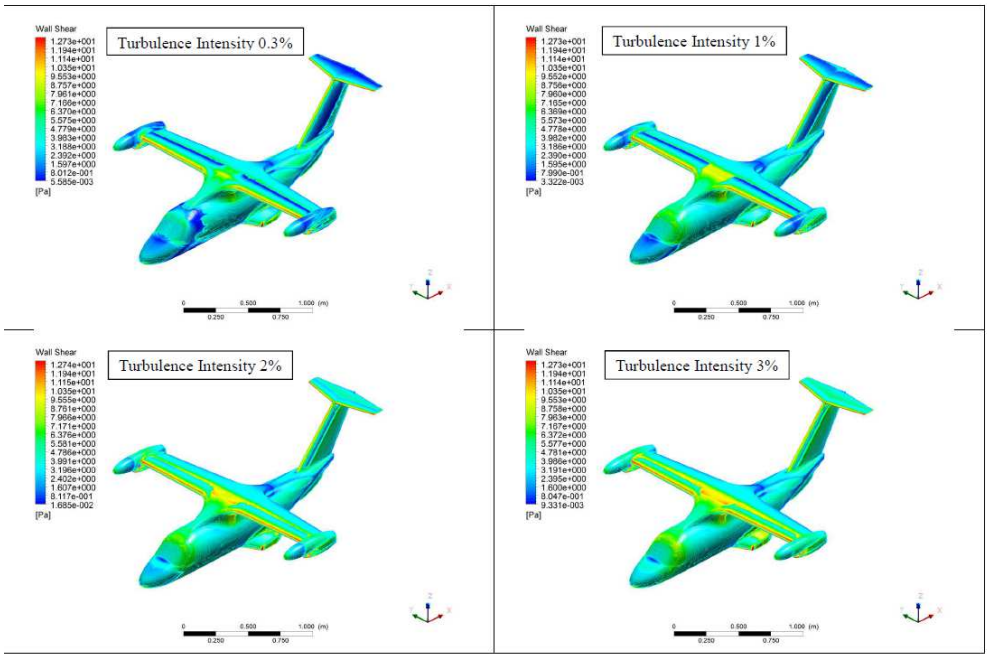

Figure 17: Simulations of laminar/turbulent transition over the 1/8th scaled model @ a=-1.89 deg: assessment of turbulence intensity effects on transition location and aerodynamic coefficients.

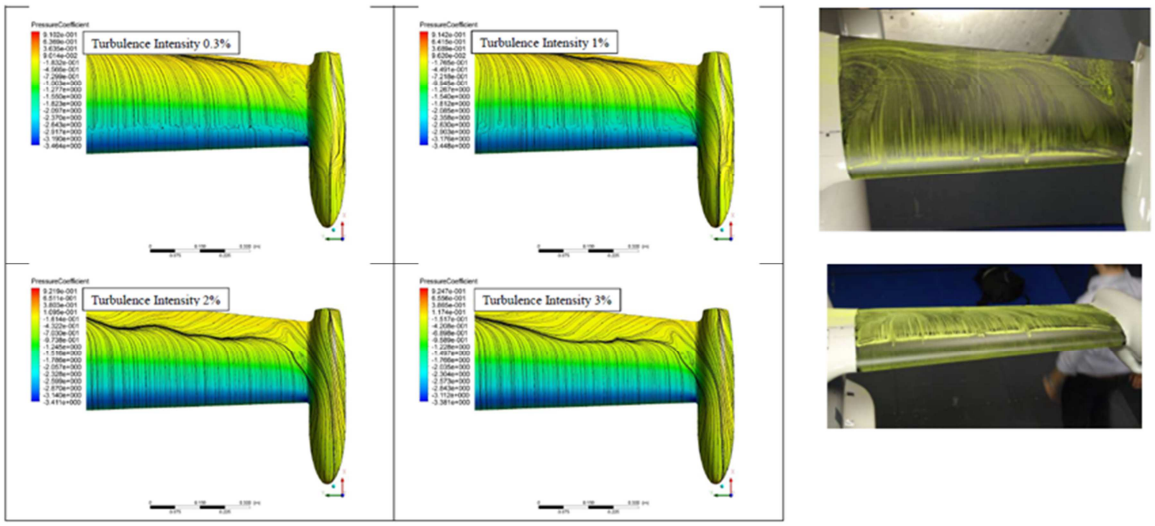

Figure 18: Simulations of laminar/turbulent transition over the 1/8th scaled model @ a=+10 deg: Assessment of turbulence intensity effects on transition location over the wing and comparison with experimental flow visualization.

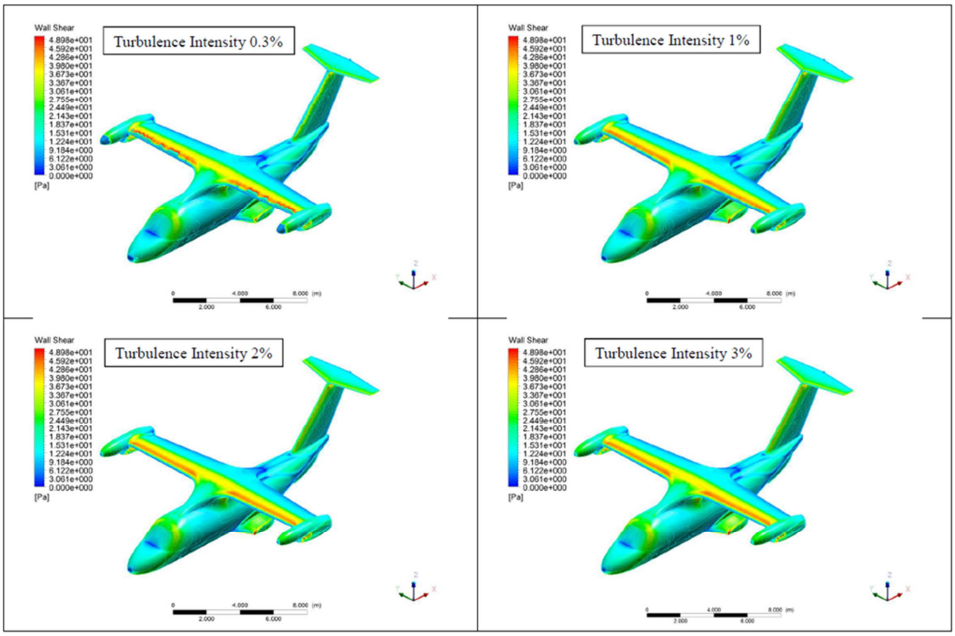

Figure 19: Simulations of laminar/turbulent transition over the full scale model @ a=-1.97 deg: Assessment of turbulence intensity effects on transition location and aerodynamic coefficients.

Optimization effects assessment at full scale conditions

The numerical models already set-up and validated against wind tunnel data (over the 1/8 model scale aircraft) were used to assess the aerodynamic performance of the full scale fuselage, both with and without inclusion of rotor effects. In particular, the rotor effects were included in the numerical simulations using an actuator disc approach. Once again, all the intermediate optimized configurations, obtained mounting the optimized components one at a time on the baseline fuselage, were assessed in order to derive an accurate analysis of the effects of shape optimization of various components on the aircraft performance at Mach and Reynolds numbers typical of the full scale operating conditions. First of all, the simulations over the baseline geometry at full scale conditions were analysed, and results were compared against those on the $1/8^{th}$ scaled model. Then, all the intermediate optimized configurations were analysed and the obtained numerical results were assessed in terms of global aerodynamic coefficients. All the modifications and drag improvements coming from the inclusion of optimised components were monitored. In a second stage, also the effects of rotor inclusion were accounted for and their influence on optimised components was assessed.

The following results were found:

1. for the baseline geometry at full scale conditions, it was found that the slope of lift curve was increased with respect to the scaled model due to increased Mach and Reynolds number (even though this effect was partially counterbalanced by geometrical differences in wing/fuselage fairing); on the other hand, drag at optimization attitude was decreased with respect to the scaled model; moreover, inclusion of rotor effects has negligible impact on the aerodynamic coefficients, at least over a range of incidence angles next to the optimization one;
2. regarding the ***nose***, results obtained at full scale without rotor effects are consistent with those coming from the component optimization. Specifically, a drag reduction is achieved thanks to the optimized nose (even though it is smaller than the reduction originally obtained from the component optimization), accompanied with a simultaneous lift increase. At α =-1.97 deg, which is the incidence value used for optimization, the drag reduction is equal to 0.23%, with a

simultaneous lift increase of 0.54%. On the other hand, when rotor inflow is included, the beneficial effect of nose optimization found without rotors seems to be cancelled, while lift is preserved. It follows that also the aerodynamic efficiency is not enhanced due to the introduction of the optimized nose.

3. as far as the optimized ***wing/fuselage junction*** is concerned, at full scale conditions and without rotors it gives a drag reduction at incidences equal to the cruise value. However, this drag reduction is accompanied with a simultaneous lift decrease. In particular, at α =-1.97 deg, the drag reduction is equal to 0.65%, with a simultaneous lift decrease of 4.65%. Regarding the aerodynamic efficiency, no significant differences are introduced as per the optimized wing/fuselage junction with respect to the configuration with optimized nose, at least in the region near the optimization attitude. Results obtained in wind tunnel conditions are consistent with those coming from the component optimization. Actually, a lift decrease was found also during optimization at full scale conditions, but it was decided to accept it, since solutions that did not penalized lift featured smaller drag reduction than the finally selected one, which was in fact capable of maximizing drag reduction. On the other hand, when rotor inflow is included, the optimized wing/fuselage junction still has a beneficial effect. In particular, a reduction of drag equal to 0.88% is achieved with respect to the fuselage with only optimized nose and a lit decrease of 4.13%. Hence, inclusion of rotor effects seems to amplify the benefits in drag reduction with respect to the case without rotor, and it is also beneficial in terms of reduction of lift penalization. It follows that the aerodynamic efficiency is slightly increased due to the introduction of the optimized wing/fuselage junction.
4. concerning the optimized ***sponson***, a significant drag reduction, equal to 4.03% was found at cruise attitude and full scale conditions, together with a slight lift reduction, equal to 0.31%. A meaningful enhancement was also found in the aerodynamic efficiency. These results are nearly consistent with those coming from the component optimization, even though drag reduction there was higher than the current result. When the rotor effects are taken into account, the inclusion of optimized sponson still has a significant beneficial effect, even though smaller than the case without rotor included. In particular, a reduction of drag equal to 2.74% is achieved with respect to the fuselage with only optimized nose and wing/fuselage junction and a lit decrease of 1.26%. Hence, inclusion of rotor effects seems to penalize the benefits in drag reduction pertinent to the optimized sponson without rotor, and it is also detrimental in terms of lift penalization. In any case, the aerodynamic efficiency is increased due to the introduction of the optimized sponson, even though enhancement is less than predicted without rotors.
5. regarding the optimized ***empennage***, a drag increase of 0.26% was found at cruise attitude without rotor inclusion, together with a lift decrease equal to 1.51%. These results are not consistent with those coming from the component optimization, since the drag penalization was obviously not found during optimization, being the drag reduction the main objective of optimization. On the other hand, when the rotor effects are taken into account, the inclusion of optimized empennage has a beneficial effect in terms of both drag reduction and minimization of lift penalization. In particular, a reduction of drag equal to 0.65% is achieved with respect to the fuselage with only optimized nose, wing/fuselage junction and empennage and a lit decrease of 0.37%. Hence, inclusion of rotor effects seems to bring back in the right direction the effects of empennage optimization. This implies that also the aerodynamic efficiency is slightly improved, at least at optimization attitude.

The simulation results of the fully optimized fuselage (i.e. fuselage with optimized nose, wing/fuselage

junction, sponsons and empennages) at full-scale conditions are reported in Figure 20 and compared against the baseline. A zoom of the curves near the optimization attitude (i.e. α=-1.97 deg) is shown in the same figure. It is apparent that a significant drag reduction is achieved for -18 deg<α<4 deg. In particular, for α close to the optimization attitude, a drag reduction equal to 4.5% is achieved thanks to the optimized components (percentage values are referred to the overall aircraft without propeller stubs). However, this drag reduction is accompanied with a simultaneous lift decrease, mainly due to the wing/fuselage junction, and partially also to the empennage. In particular, at α=-1.97 deg, the lift decrease amounts to 6% approximately.

In addition, from Figure 8 it is apparent that the linear portion of the lift curve is slightly shifted downward in the vicinity of the optimization attitude, even though its slope is left nearly unchanged. Despite the lift decrease, it is worth noting that the aerodynamic efficiency of the optimized fuselage is significantly increased with respect to the baseline, over a range of incidence angles close to the optimization one. Finally, regarding the pitching moment characteristics, the linear portion of the curve is shifted upwards with respect to the baseline, and its slope is slightly decreased.

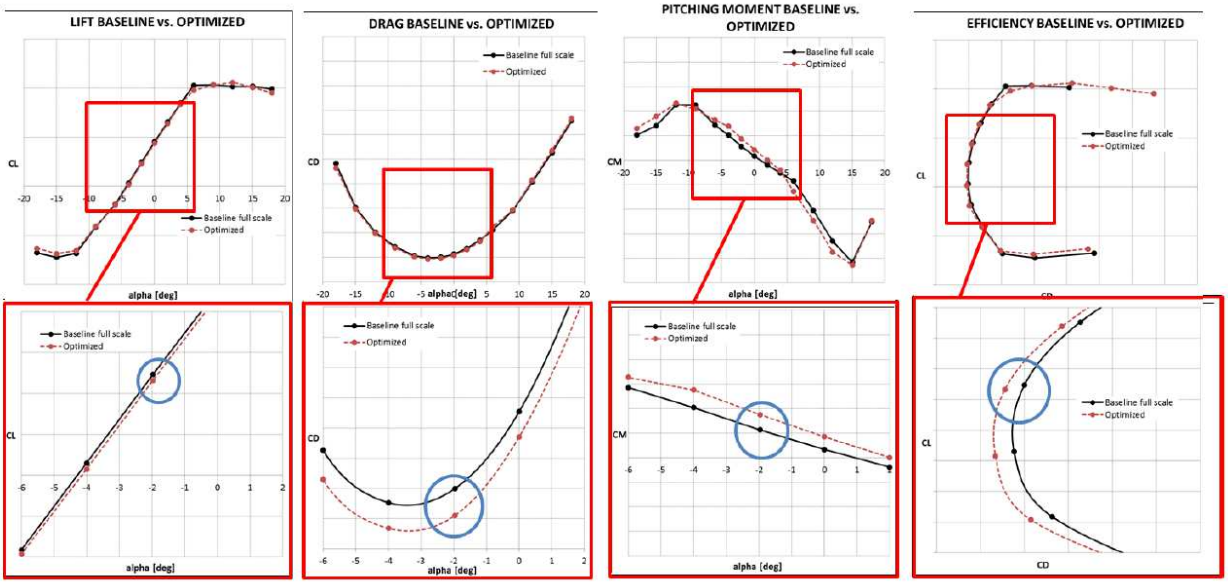

Figure 20: Lift, drag and pitching moment polars and efficiency curve of the full-scale optimized geometry compared against the baseline. Overall polars (top) and zoom around the optimization attitude (bottom).

In Figure 21, a summary of the achieved optimization results in terms of drag reduction is given: in particular, CODE-Tilt and DREAm-TILT results for each optimized component are reported and compared against the pertinent GRC target and the results over the 1/8th scaled model (both numerical and experimental). First of all, it is worth underlining that the original drag reduction calculated in the CODE-Tilt project refers to the aircraft without rotor stubs: since stubs contribute to the whole drag in a significant way (approximately 30% of the total drag), and since they were actually included in the wind tunnel tests, the drag gain coming from optimization was recalculated including stubs. As apparent from Figure 21, while without stubs the achieved reduction in CODE-Tilt was 7.7%, including the stubs it is reduced to 5%. On the other hand, in the present work, it was found that the overall drag reduction at design incidence and full-scale conditions is equal to 4.5% ca. (not including stubs and rotor). Drag reduction is lowered at 4.2% when rotors are included. In any case, inclusion of rotors seems to preserve the majority of the beneficial effects coming from optimized components. The inconsistencies with the original findings from the optimization (in particular with regard to the empennage contribution) could be due to differences in the numerical

model set-up (especially regarding the computational grid). Also, during optimization one optimized component at a time was taken in consideration and optimization of each component was carried out with all the other components in their baseline version. Hence, no interference effects among optimized components were considered. These effects are included in the CFD simulations at full-scale conditions. Therefore, this could be an additional explanation for the differences observed here with original values coming from components' optimization, especially for empennages, that are located downstream of all the modified components.

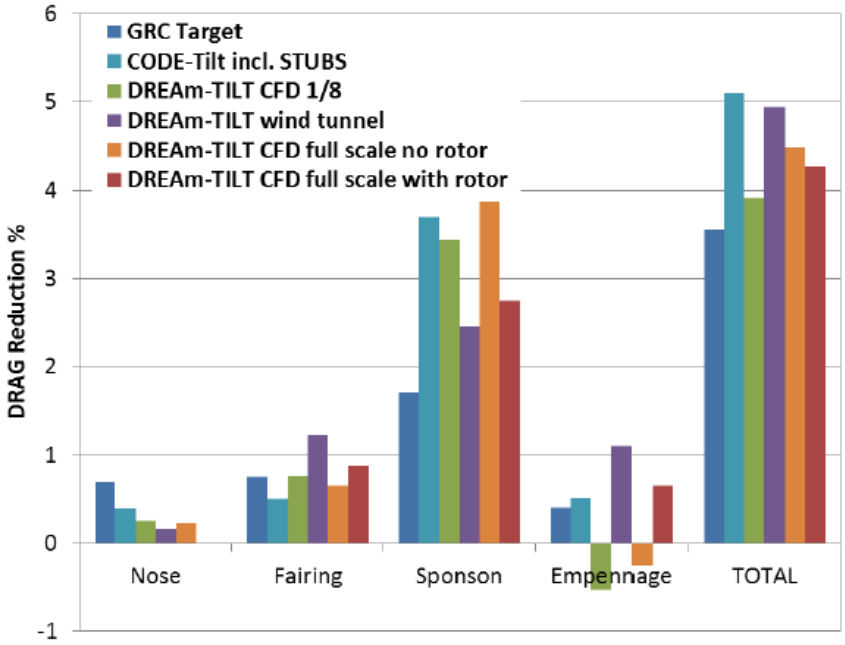

Figure 21: Summary of achieved optimization results at full scale conditions in terms of drag reduction: CODE-Tilt and DREAm-TILT results vs. GRC target, numerical and experimental results.

Numerical simulations of tiltrotor fuselage using the open-source code OpenFOAM®

A comparative study was carried out aimed at assessing the CFD open-source code OpenFOAM® capabilities over the tiltrotor fuselage. Specifically, a series of simulations both on the 1/8 scaled model and on the full scale fuselage at typical operative flight conditions were carried out and CFD results were compared against both experimental data and Fluent® calculations performed previously.

Regarding simulations of the baseline 1/8 scaled model, correlation of aircraft aerodynamic polars between OpenFOAM® and both experimental data and Fluent® results was very good, especially at low and medium angles of attack (Figure 22). In particular, CL and CD values are captured with high accuracy at the optimization incidence. In addition, also the aerodynamic efficiency curve very well correlated with experimental values.

Moreover, the static pressure distributions over the fuselage and total pressure losses downstream of it calculated using OpenFOAM® compared very well with those simulated with Fluent® throughout the whole range of incidence angles (Figure 23).

Also regarding the effects of optimized components, OpenFOAM® was able to capture them very satisfactorily. Actually, the comparison with both wind tunnel data and Fluent® results is very good, as apparent from Figure 24.

OpenFOAM® reliability in simulating the tiltrotor fuselage was confirmed also in the case of the full scale configuration with increased values of both Reynolds and Mach numbers, even if a small increment of the OpenFOAM® numerical instabilities was registered.

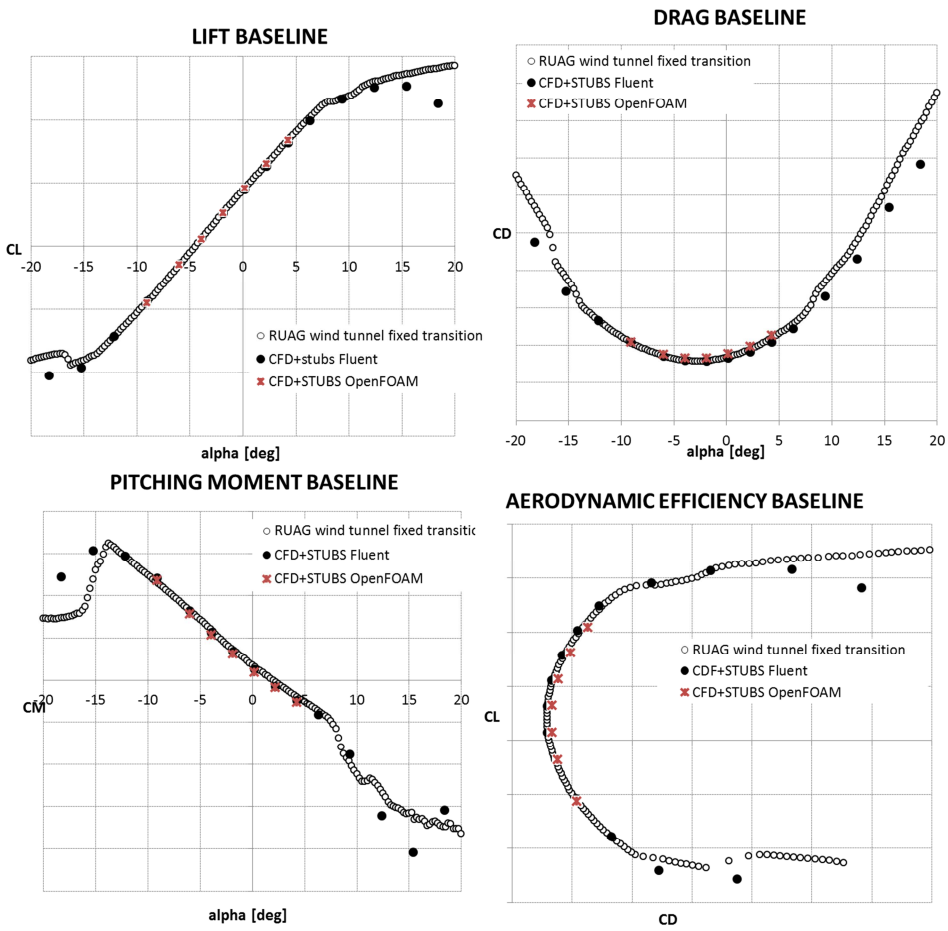

Figure 22: Baseline 1/8 scaled fuselage simulations using OpenFOAM®: comparison against wind tunnel data and Fluent® results.

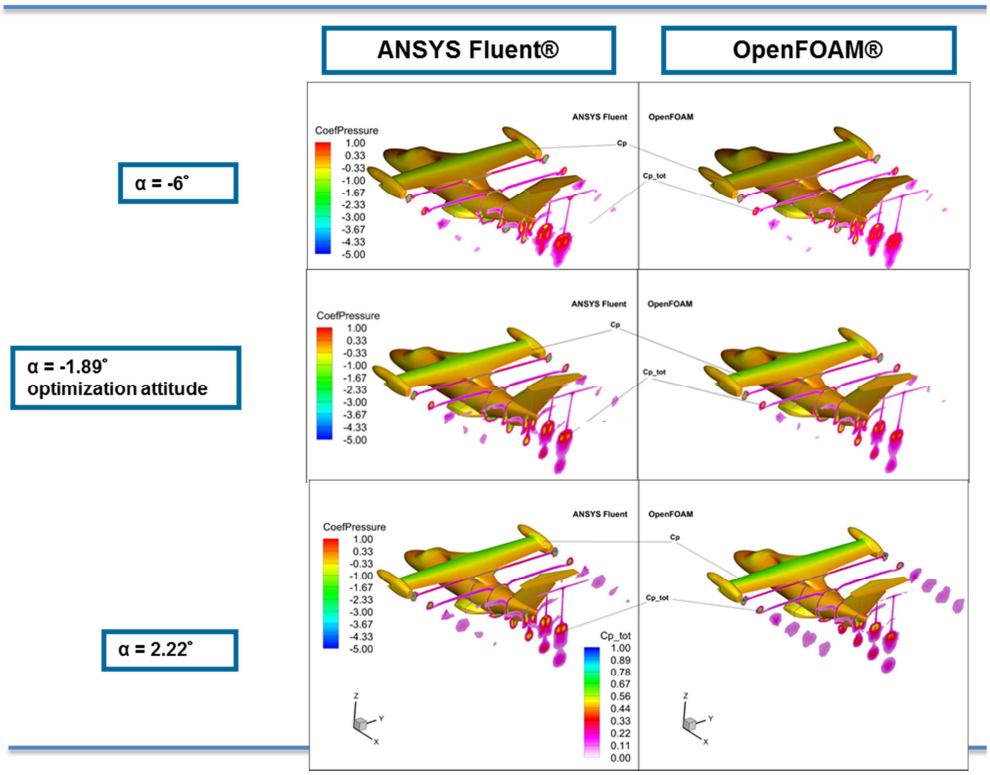

Figure 23: Model scale simulations, baseline geometry: comparison of pressure coefficient contours &total pressure losses obtained from Fluent® and OpenFOAM® at various attitudes.

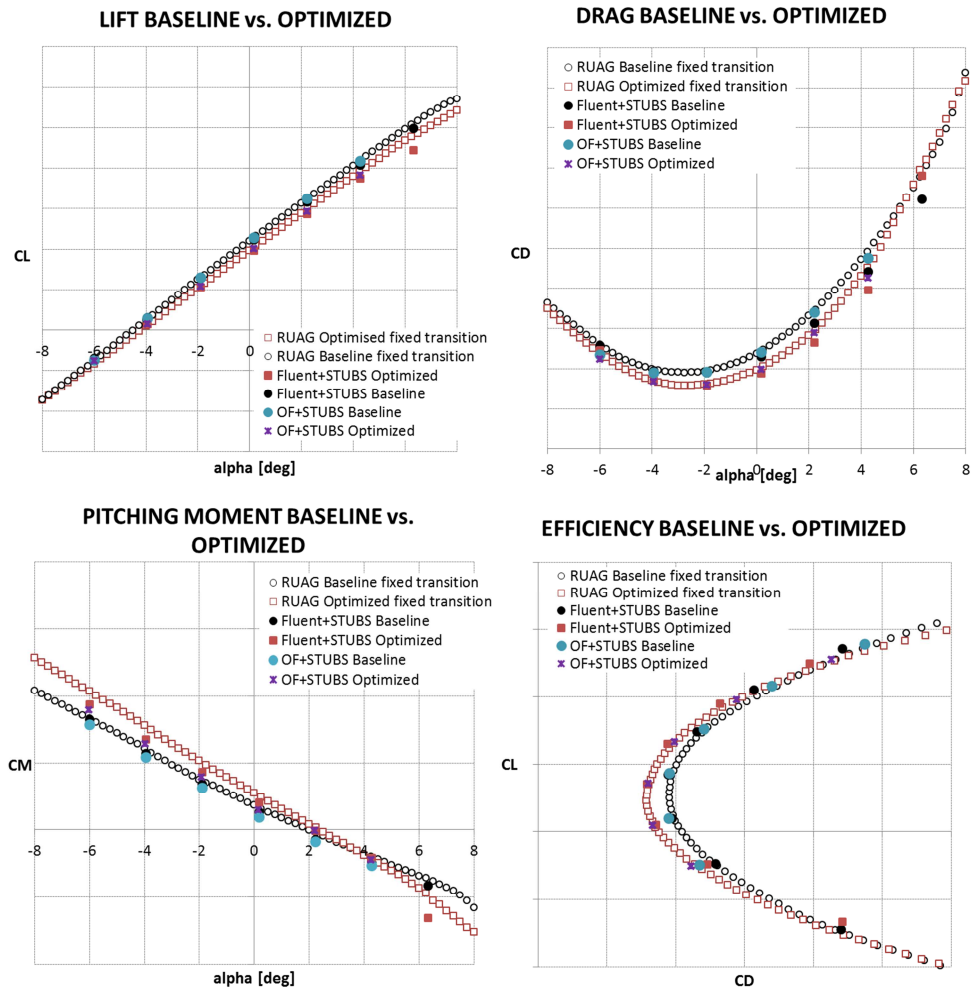

Figure 24: Simulations in wind tunnel conditions using OpenFOAM®: optimized vs. baseline fuselage and comparison against both wind tunnel data and Fluent® results.

Main conclusions of the DREAm-TILT project

The major conclusions of the DREAm-TILT program are summarized in the following:

- passive shape optimization effects of some critical ERICA fuselage components (i.e. nose, w/f junction, sponsons and empennage) were assessed by means of Wind Tunnel tests at RUAG facilities. State-of-the-art measurement techniques (i.e. IR Thermography, Minitufts visualization and PIV) were applied for a thorough characterization of the aerodynamic performance of the fuselage components;
- the CFD models on the 1/8 scaled model of ERICA tiltrotor were fully validated against RUAG wind tunnel data over a wide range of angles of attack: an excellent correlation was found and the effects of geometry modifications were captured with high accuracy, exception given for the empennage;
- overall drag reduction on scaled model at wind tunnel conditions was equal to 4.9% (WT) or 3.93% (CFD), with a simultaneous lift decrease of 15.6% (WT) or 17.3% (CFD). The main responsible for lift reduction is the optimized wing/fuselage junction (already present in the baseline fuselage used for optimization);
- the largest contribution to drag reduction comes from the optimized sponsons, followed by the optimized wing/fuselage fairing;

- wind tunnel drag reduction is consistent with CODE-Tilt results; the target required by GRC (-3.5%) achieved and exceeded (according to both CFD and wind tunnel);
- the wakes from the sponson (both baseline and optimised) were characterised by Stereo PIV measurements: alleviation of the wake for the optimized sponson was found to be between 15 to 30 counts, and an out of plane vorticity reduction between 20% and 35% was registered;
- PIV and CFD data comparison is still under processing, preliminary results indicates that full geometry and unsteady calculations are necessary;
- the validated CFD models were used for simulations at full scale conditions, including rotor effects;
- the achieved overall drag reduction at full scale conditions and design incidence was -4.49% (without rotor) and -4.20% (with rotor);
- also in this case, the target required by GRC (-3.5%) was achieved and overcome, even though the reduction smaller than predicted in CODE-Tilt;
- a lift decrease of 5.87% (without rotor) and 6.58% (with rotor) was registered as well: this reduction is due to w/f junction and partly to empennages;
- nevertheless, a meaningful enhancement of aerodynamic efficiency was achieved;
- the pitching moment is slightly modified by nose and empennages, but it is still considered to be manageable. Hence, no meaningful stability issues arise, which was an important issue during optimization;
- on the whole, beneficial effects of optimized components at full scale were demonstrated;
- in general, multi-objective evolutionary optimization techniques coupled with CFD tools were demonstrated to be mature enough for product application (excellent agreement with Wind Tunnel results reinforces the confidence in the numerical design tool): TRL4 was achieved.